

Photoinduced Phase Transition of Diamond: A Nonadiabatic Quantum Molecular Dynamics Study

Shogo Fukushima, Nabankur Dasgupta, Rajiv K. Kalia, Aiichiro Nakano,* Kohei Shimamura, Fuyuki Shimojo, and Priya Vashishta



Cite This: *J. Phys. Chem. Lett.* 2025, 16, 9267–9272



Read Online

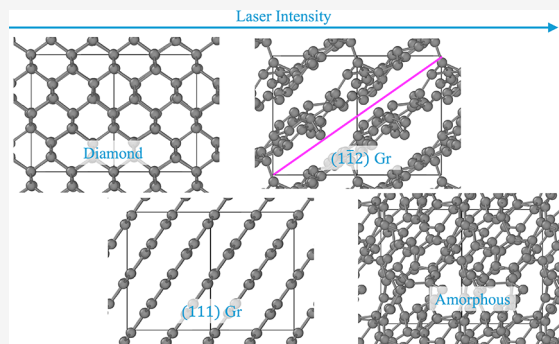
ACCESS |

Metrics & More

Article Recommendations

Supporting Information

ABSTRACT: Photoinduced phase transition holds the key to realizing novel states of matter and transition pathways that do not exist otherwise. An example is ultrafast graphitization of diamond using femtosecond soft X-ray laser pulses, for which the structural transformation pathways have not been fully explored. Using first-principles nonadiabatic quantum molecular dynamics simulations, we found a progression from order-to-order (diamond-to-graphite) to order-to-disorder (diamond-to-amorphous) phase transitions at elevated laser intensities. We further found a novel graphitization pathway on the crystallographic $(\bar{1}\bar{1}2)$ plane at high intensities below the order-to-disorder intensity threshold, which is distinct from the common $(1\bar{1}1)$ -graphitization mechanism in thermal and low-intensity photopathways. This study reveals rich coexistence of phase-transition pathways under intense irradiation, thus expanding the notion of ultrafast laser control of material phases.



Light-matter dynamics in materials holds promise for ultrafast control of materials on demand.¹ Nonlinear interaction of laser light with matter generates attosecond (10^{-18} s) pulses.² The new era of attosecond physics was heralded by the 2023 Nobel physics prize to Agostini, Krausz, and L'Hullier. It has been demonstrated that nonequilibrium structural-transformation pathways can be controlled by tuning ultrafast laser pulses.³ Irradiation of matter with a femtosecond laser pulse commonly induces structural transition to a disordered state, such as amorphization, or creation of defects.⁴ Photoinduced graphitization of diamond is a counterexample, as it is an order-to-order (solid-to-solid) phase transition.⁵

Photoinduced graphitization was experimentally observed by applying soft X-ray pulses to diamond.^{6,7} In one experiment, the wavefront of a free-electron laser (FEL) was tilted with respect to the target; thus the integrated FEL fluence is encoded spatially and temporally onto the surface of the target.⁶ The graphitization process was also investigated by computer simulations based on a tight-binding model.^{8–12} In one simulation, the system transformed from diamond to graphite structures within 500 fs after irradiation with a soft X-ray pulse of 47.4 eV photon energy, where carbon atoms were displaced on crystallographic $(1\bar{1}1)$ planes of diamond.⁶ The authors concluded that the energy delivered to the system by incoming photons led to a change in the interatomic bonding from sp^3 to sp^2 characters, causing the diamond-to-graphite transition.

In another study using molecular-dynamics (MD) simulations based on a tight-binding model,¹³ graphitization was

observed within 100 fs by increasing the electronic temperature. The phase transition was observed to occur on the $(1\bar{1}1)$ planes of diamond. The study showed that graphitization of diamond can also occur thermally through the temperature of atoms, in addition to a nonthermal process driven by the change in the energy landscape due to electronic excitation by a laser pulse. In their study, graphitization also occurred by the change of interatomic bonding from sp^3 to sp^2 . However, how photoexcitation causes such a bond change remains elusive.

In this study, we study microscopic mechanisms of photoinduced graphitization using first-principles nonadiabatic quantum molecular dynamics (NAQMD) simulations;^{14–16} see the *Methods* section for details.

To confirm that the optical absorption spectrum of diamond is reasonably described by the simulation method, we first calculate the oscillator strength defined as^{17,18}

$$\mathcal{F} = \frac{mE_{\text{exc}}}{2\hbar^2} \left| \int d\mathbf{r} \psi_e^*(\mathbf{r}) \frac{\nabla \cdot \mathbf{e}}{i} \psi_h(\mathbf{r}) \right|^2 \quad (1)$$

where E_{exc} is the optical excitation energy, ψ_e is the electronic wave function at the conduction-band edge, ψ_h is the hole wave

Received: May 2, 2025

Revised: August 22, 2025

Accepted: August 25, 2025

function at the valence-band edge, e is the unit vector parallel to the polarization of incident light, \hbar is the Planck constant, and m is the electron mass. Figure 1 shows the calculated oscillator strength of the diamond. Because of the peak at $E_{\text{exc}} = 40$ eV, the photons with energy around 40 eV can be efficiently absorbed in diamond.

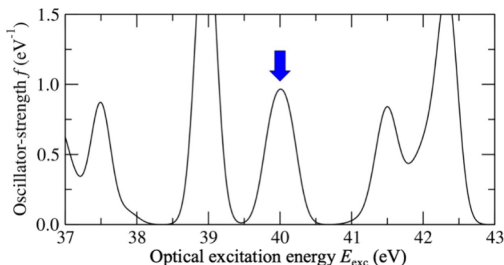


Figure 1. Calculated oscillator strength of diamond.

We perform NAQMD simulations using the excitation energy $E_{\text{exc}} = 40$ eV, where 3% of the valence electrons are excited. The NAQMD simulations are started after equilibrating the system under the canonical (NVT) ensemble at 300 K for 1 ps. Figure 2 shows the time evolution of (a) potential

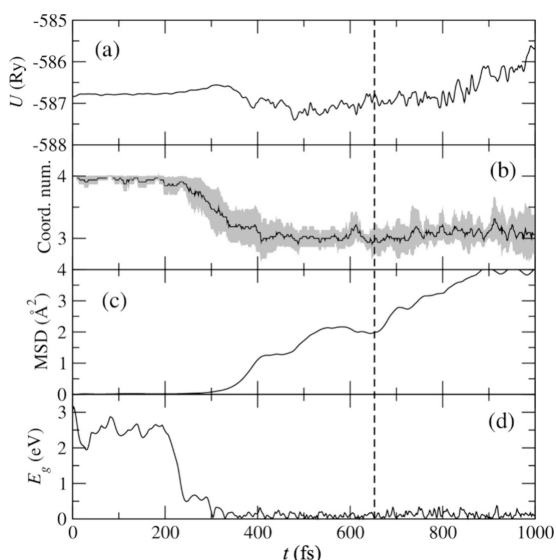


Figure 2. Time evolution of (a) potential energy, (b) coordination number, (c) mean-square displacement (MSD), and (d) bandgap. Gray area in (b) shows the standard deviation.

energy U , (b) coordination number, (c) mean-square displacement (MSD), and (d) electronic bandgap E_g . All four quantities maintain the respective initial values for 200 fs after photoexcitation at time 0, then change systematically during 200–400 fs. The potential energy first increases slightly from 200 to 300 fs, then decreases by 0.4 Ry (Figure 2a). The coordination number changes from 4 to 3, which shows the change of bond character of carbon atoms from sp^3 to sp^2 . The MSD increases at 300 fs and remains at a steady value until 650 fs. This indicates that the structure has transformed at 300 fs, which is maintained until 650 fs. The bandgap decreases from 3 to 0 eV. While the initial bandgap, 3 eV, of diamond is underestimated by the generalized gradient approximation (see Methods), the final bandgap of 0 eV clearly represents the bandgap of graphite. These results show that the structure has

transformed from diamond to graphite. After 650 fs, the potential energy and MSD increase, whereas the coordination number fluctuates greatly, which indicates that the structure has collapsed likely due to the large energy deposited to the system.

Figure 3a,b shows snapshots of the system at times 0 and 550 fs, respectively. The diamond structure is maintained for 200 fs after photoexcitation. Subsequently, the structure starts transforming and converges to the graphite structure around 550 fs with the cubic supercell. The obtained graphite structure has a stack of graphene planes parallel to the crystallographic $(\bar{1}\bar{1}2)$ plane as shown in Figure 3b. Figure 3c shows one of the graphene sheets at 550 fs projected along the direction perpendicular to the graphene plane. Red, blue, and gray area in Figure 3c show 7-, 5-, and larger-than-8-membered rings, respectively. These non-six-membered rings are structural defects that are commonly observed in experimental study. In previous simulations, diamond-to-graphite transformation involved graphene planes on the crystallographic (111) plane of diamond.^{8–10,13} Our result indicates a possibility that photoinduced graphitization pathways are not unique.

To study the effects of excitation intensity, we perform additional NAQMD simulations using other percentages of excited electrons, $n = 1, 2, 5\%$. Figure 4 shows the time evolution of (a) the potential energy and (b) the bandgap. Red, green, black, and blue lines represent the excitation percentage $n = 1, 2, 3$, and 5%, respectively. When $n = 1$ and 2%, the potential energy and bandgap keep the initial value, which indicates that structural transition has not occurred. This is confirmed by snapshots of atomic configuration in Figure 5a,b. For $n = 5\%$, bandgap rapidly decreases to 0 eV as for $n = 3\%$. However, the potential energy increases after 400 fs, without decreasing by 0.2 Ry, as for $n = 3\%$. This result indicates that the structure has transformed to a disordered state with the highest excitation energy, as shown in Figure 5d. To summarize, the threshold excitation percentage for structural transition to graphite lies between 2 and 3%, while structural to disordered states occurs when $n \geq 5\%$.

Graphitization Mechanisms. As shown in ref 13, thermal diamond-to-graphite pathways involve (111) graphene planes. In a longer time at low electronic excitation, a similar (111) mechanism is expected instead of the high-excitation $(\bar{1}\bar{1}2)$ mechanism shown in Figure 3b.

Six-membered rings exist on the (111) planes in the diamond structure. In fact, graphitization was observed on (111) planes in previous studies.^{8–10} Figure 6 shows a schematic of an ideal mechanism on (111) planes, which we refer to as (111) -graphitization. The graphitization mechanism on (111) planes is very simple as follows:

1. Cut the bonds parallel to the $[111]$ direction, which we refer as $[111]$ -bonds.
2. Compress vertically to the (111) plane.

Graphitization on $(\bar{1}\bar{1}2)$ planes (referred to as $(\bar{1}\bar{1}2)$ -graphitization) was observed instead in our NAQMD simulations. To create 6-membered rings on planes other than (111) , cutting of C–C bonds other than $[111]$ -bonds is required, along with rebonding with another layer. For example, in the case of $(\bar{1}\bar{1}2)$ plane, a possible mechanism is as follows (see Figure 7):

1. Cut not only $[111]$ -bonds but also bonds on (111) planes.

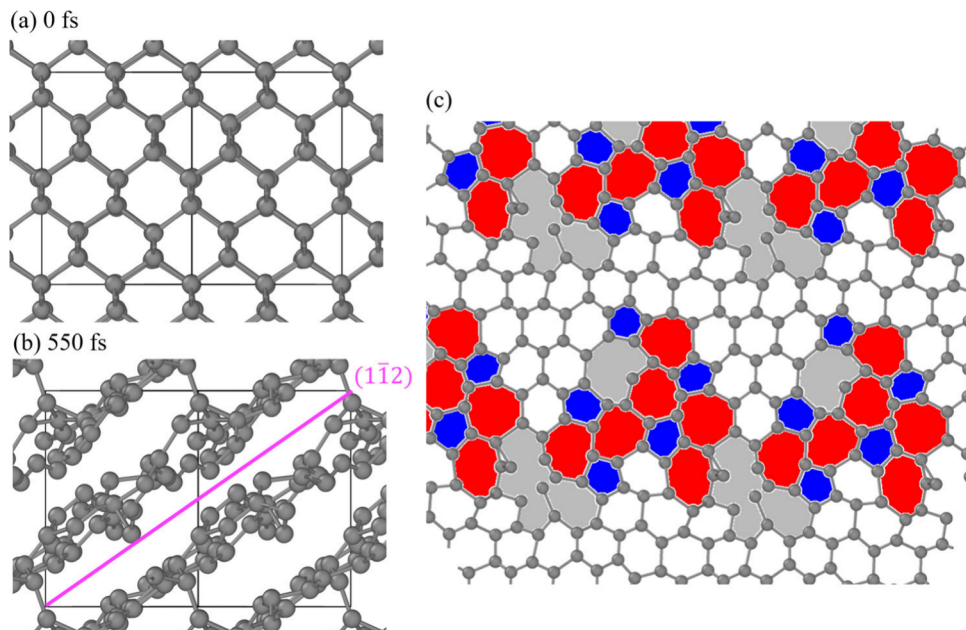


Figure 3. Snapshots of the system at (a) 0 fs and (b) 550 fs in the [110] projection and (c) obtained graphene structure at 550 fs in the projection perpendicular to the graphene plane. Red, blue, and gray areas in panel (c) are 7-, 5-, and larger-than-8-membered rings, respectively.

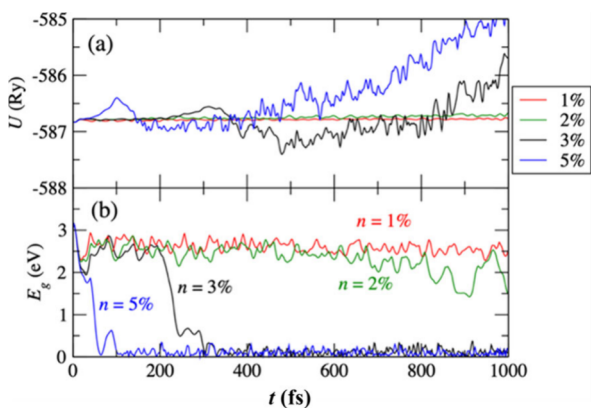


Figure 4. Time evolution of (a) potential energy and (b) electronic bandgap. Red, green, black, and blue lines represent the excitation percentage $n = 1, 2, 3, 5\%$, respectively.

2. Slide yellow-colored atoms in Figure 7 in half-period of the crystal structure in the [110] direction.
3. Cut bonds perpendicular to $[1\bar{1}2]$.
4. Compress in the $[1\bar{1}2]$ direction.

Figure 7 shows a schematic of the mechanism of $(\bar{1}\bar{1}2)$ -graphitization. The process from (a) to (b) is sliding of yellow-colored atoms in the half-period of the crystal structure in the [110] direction, which corresponds to steps 1 and 2 described above. The process from (b) to (c) is compression in the $[1\bar{1}2]$ direction, which corresponds to steps 3 and 4 described above. The number of cut bonds in $(\bar{1}\bar{1}2)$ -graphitization is larger than that in (111) -graphitization. Therefore, the energy barrier of $(\bar{1}\bar{1}2)$ -graphitization is larger than that of (111) -graphitization, i.e., (111) -graphitization can occur more easily than $(\bar{1}\bar{1}2)$ -graphitization. We thus expect the $(\bar{1}\bar{1}2)$ -graphitization mechanism to operate under higher laser intensities.

In summary, we have investigated atomistic mechanisms of photoinduced graphitization of diamond using NAQMD

simulations. We found diamond-to-graphite-to-amorphous transitions for increased numbers of excited electrons. To demonstrate the robustness of this finding with respect to the photon energy, we have performed additional NAQMD simulation using a different excitation energy of $E_{exc} = 47.4$ eV. The results shown in Figures S4–S6 in the Supporting Information indeed confirm these transitions. Graphitization observed in the NAQMD simulations involves graphene planes parallel to the $(\bar{1}\bar{1}2)$ crystallographic plane of diamond, which is different from a common graphitization mechanism involving the (111) plane in thermal and low-intensity-photo structural transformation pathways. This study thus indicates a possibility that photoinduced graphitization mechanism is not unique, involving other crystallographic planes than (111) , under intense irradiation just below the order-to-disorder transformation threshold. In fact, NAQMD simulations of a larger system size shows a mixture of $(\bar{1}\bar{1}2)$ and (111) graphitization planes (see Figure S7 in the Supporting Information), thereby confirming rich photoinduced phase transition pathways. Detailed statistics of multiple transition pathways will be an important future topic.

METHODS

To study photoexcitation dynamics involving electrons and nuclei, we perform nonadiabatic quantum molecular dynamics (NAQMD) simulations.^{14–16} The NAQMD method numerically solves time-dependent Kohn–Sham (KS) equations in the framework of time-dependent density functional theory (TDDFT)¹⁹ to describe time-evolution of electronic wave functions, subjected to nuclei motions through nonadiabatic coupling (NAC) within the surface-hopping (SH) approach.^{14–16} In SH-NAQMD, electronic excitation states are represented in terms of the ground-state KS orbitals $|\phi_{s\sigma}\rangle$ (s and σ are orbital and spin indices) and their occupations $f_{s\sigma} \in \{0,1\}$. We perform SH-NAQMD simulations for 1000 fs using a unit time-step of 1 fs. We consider four different initial occupations where 1, 2, 3, and 5% of the valence electrons are excited, respectively.

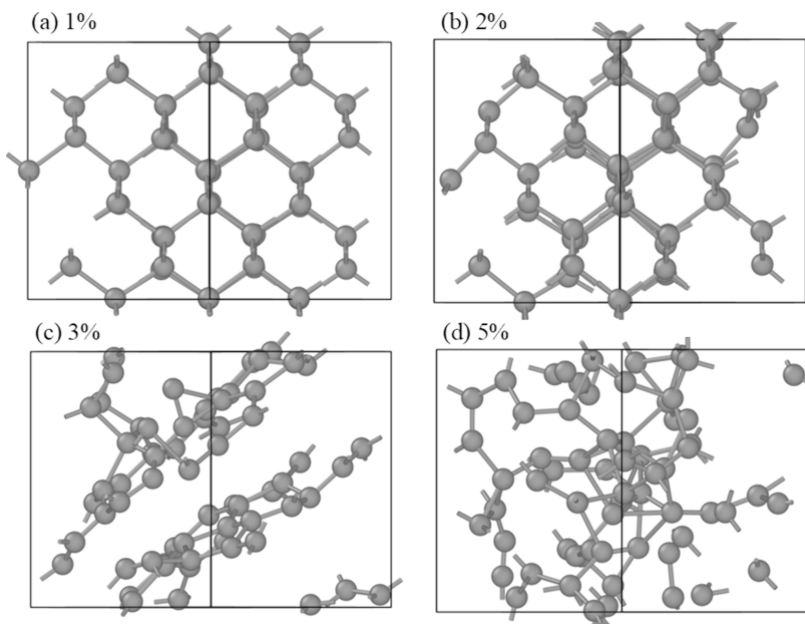


Figure 5. Snapshots of atomic configuration at 550 fs using excitation percentage of n = (a) 1, (b) 2, (c) 3, and (d) 5%. The systems (a) and (b) maintain the original diamond structure, (c) have transformed to graphite, and (d) have transformed to a disordered state.

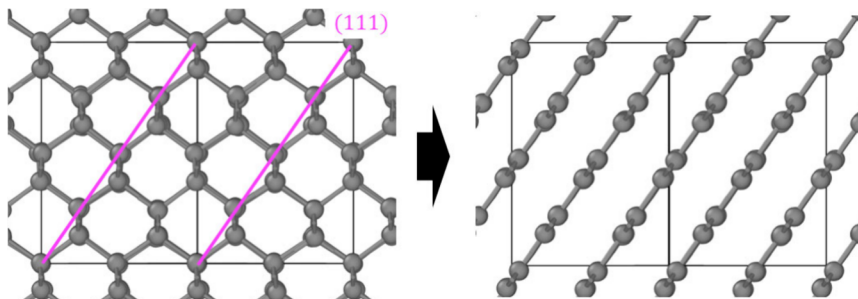


Figure 6. Schematic of an ideal graphitization mechanism on (111). Magenta lines show the (111) planes. When all carbon atoms are compressed in the [111] direction, a graphite structure is obtained.

To guide the amount of electronic excitation, we simulate an experimental laser pulse⁶ (photon energy, 47.4 eV; pulse duration, 52.5 fs; fluence 18 J/cm²) using the Maxwell–Ehrenfest (ME) NAQMD method.^{20–23} Here, Maxwell's equations for light are solved concurrently with TDDFT equations for electrons to obtain KS wave functions $|\psi_{s\sigma}(t)\rangle$ as a function of time t , starting with the ground-state occupations $f_{s\sigma}^{(0)}$ and $|\psi_{s\sigma}(0)\rangle = |\phi_{s\sigma}\rangle$. We then remap $|\psi_{s\sigma}(t)\rangle$ to fractional occupations of $|\phi_{s\sigma}\rangle$ as

$$f_{s\sigma}(t) = \sum_u |\langle \phi_{s\sigma} | \psi_{u\sigma}(t) \rangle|^2 f_{u\sigma}^{(0)} \in [0, 1] \quad (2)$$

and the number of excited electrons as

$$n_{\text{exc}}(t) = \sum_{s\sigma \in \text{occupied}} (f_{s\sigma}^{(0)} - f_{s\sigma}(t)) \quad (3)$$

where the sum is taken over the initially occupied orbitals. A similar multiscale simulation approach was adopted in recent works, where electronic occupation numbers provided handshaking between ME-NAQMD to describe short-time photon or ion-beam irradiation and SH-NAQMD to describe longer-time materials response.^{22,24} Separation between ME and SH time-scales is determined by the quantum uncertainty principle as $t \sim \hbar/\Delta E$ ($\sim 10^{-15}$ s), where ΔE is the separation

between key electronic energy levels that dictate photoinduced molecular dynamics and \hbar is the Planck constant. More recently, a divide-and-conquer (DC) scheme²⁵ was used to seamlessly integrate ME-NAQMD and SH-NAQMD for electrons and nuclei, along with Maxwell's equations for light, in a single code named DC-MESH (divide-and-conquer Maxwell-Ehrenfest-surface hopping).²³ The results in the main text have been obtained by SH-NAQMD simulations, while ME-NAQMD results are presented in the *Supporting Information*.

The simulation system contains 64 carbon (C) atoms in a cubic supercell under periodic boundary conditions. The density of the system is 2.26 g/cm³, which is the graphite density. While the diamond-to-graphite transition involves volume expansion in longer time, we use the expanded volume to expedite the phase transition from the metastable diamond structure within the short simulation of 1000 fs. The electronic states are calculated using the projector-augmented wave (PAW) method,²⁶ while we use the generalized gradient approximation (GGA) for the exchange–correlation energy²⁷ and the DFT-D approach to take into account van der Waals interactions.²⁸ The momentum-space formalism is utilized, where the plane-wave cutoff energies are 20 and 200 Ry for the electronic pseudowave functions and pseudocharge density,

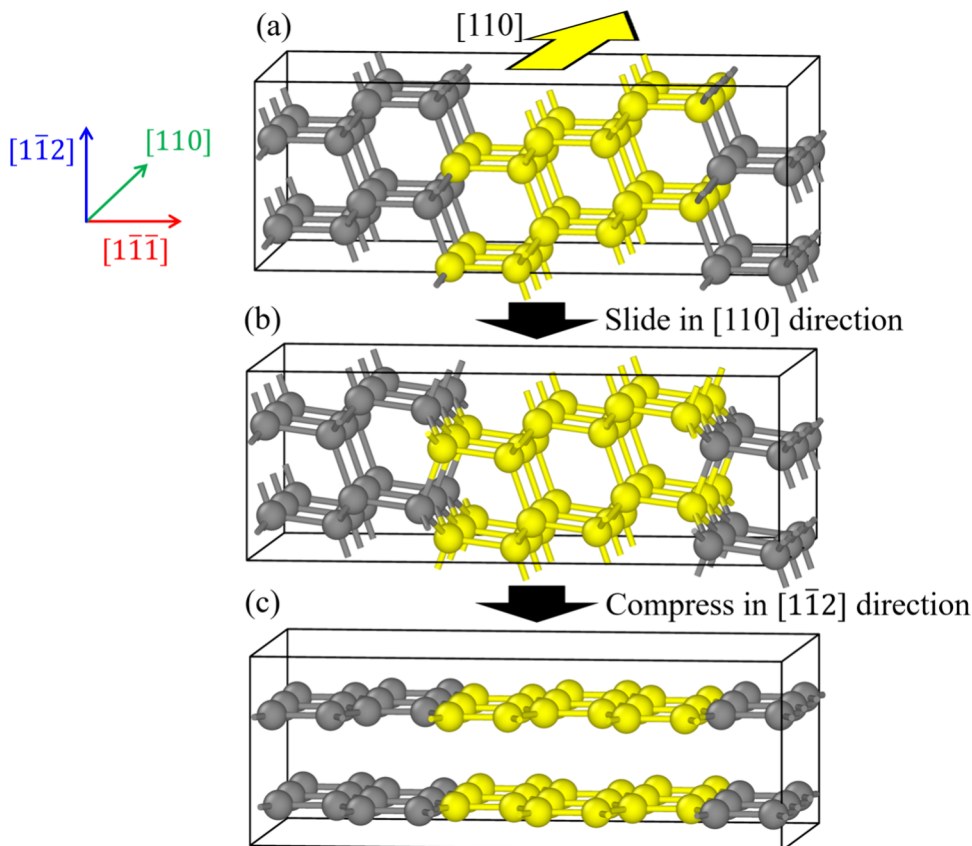


Figure 7. Schematic of the graphitization mechanism on $(1\bar{1}2)$ planes. (a) Diamond, (b) intermediate, and (c) graphite structures along the transformation pathway. The process from (a) to (b) is sliding of yellow-colored atoms in half-period of the crystal structure in the $[110]$ direction, and that from (b) to (c) is compression in the $[1\bar{1}2]$ direction.

respectively. The Γ point is used to sample the Brillouin zone. To calculate the oscillator-strength, we use the projector functions generated for 1s, 2s, and 2p states of C.

■ ASSOCIATED CONTENT

SI Supporting Information

The Supporting Information is available free of charge at <https://pubs.acs.org/doi/10.1021/acs.jpcllett.5c01332>.

ME-NAQMD simulation method, ME-NAQMD simulation results (Figures S1–S3), and additional SH-NAQMD simulation results (Figures S4–S7) ([PDF](#))

■ AUTHOR INFORMATION

Corresponding Author

Aiichiro Nakano – Collaboratory for Advanced Computing and Simulations, University of Southern California, Los Angeles, California 90089-0242, United States; orcid.org/0000-0003-3228-3896; Email: anakano@usc.edu

Authors

Shogo Fukushima – Institute for Materials Research, Tohoku University, Sendai, Miyagi 980-8577, Japan

Nabankur Dasgupta – Collaboratory for Advanced Computing and Simulations, University of Southern California, Los Angeles, California 90089-0242, United States

Rajiv K. Kalia – Collaboratory for Advanced Computing and Simulations, University of Southern California, Los Angeles, California 90089-0242, United States

Kohei Shimamura – Department of Physics, Kumamoto University, Kumamoto 860-8555, Japan; orcid.org/0000-0003-3235-2599

Fuyuki Shimojo – Department of Physics, Kumamoto University, Kumamoto 860-8555, Japan; orcid.org/0000-0002-4025-0069

Priya Vashishta – Collaboratory for Advanced Computing and Simulations, University of Southern California, Los Angeles, California 90089-0242, United States; orcid.org/0000-0003-4683-429X

Complete contact information is available at: <https://pubs.acs.org/10.1021/acs.jpcllett.5c01332>

Author Contributions

R.K.K., A.N., K.S., F.S., and P.V. designed the research. S.F., N.D., and A.N. performed NAQMD simulations. A.N. and F.S. provided simulation techniques. All authors discussed and prepared the manuscript.

Notes

The authors declare no competing financial interest.

■ ACKNOWLEDGMENTS

This work was supported by Office of Naval Research through a Multi-University Research Initiative (MURI) Grant N00014-24-1-2313. Computing was partly provided by the U.S. DOE INCITE and Aurora ESP Programs.

■ REFERENCES

- (1) Basov, D. N.; Averitt, R. D.; Hsieh, D. Towards properties on demand in quantum materials. *Nat. Mater.* **2017**, *16* (11), 1077–1088.
- (2) Krausz, F.; Ivanov, M. Attosecond physics. *Rev. Mod. Phys.* **2009**, *81* (1), 163–234.
- (3) Stoica, V. A.; Yang, T.; Das, S.; Cao, Y.; Wang, H.; Kubota, Y.; Dai, C.; Padma, H.; Sato, Y.; Mangu, A.; Nguyen, Q. L.; Zhang, Z.; Talreja, D.; Zajac, M. E.; Walko, D. A.; DiChiara, A. D.; Owada, S.; Miyanishi, K.; Tamasaku, K.; Sato, T.; Glownia, J. M.; Esposito, V.; Nelson, S.; Hoffmann, M. C.; Schaller, R. D.; Lindenberg, A. M.; Martin, L. W.; Ramesh, R.; Matsuda, I.; Zhu, D.; Chen, L.-Q.; Wen, H.; Gopalan, V.; Freeland, J. W. Non-equilibrium pathways to emergent polar supertextures. *Nat. Mater.* **2024**, *23* (10), 1394–1401.
- (4) Kudryashov, S. I.; Danilov, P. A.; Vins, V. G.; Kuzymin, E. V.; Muratov, A. V.; Smirnov, N. A.; Pomazkin, D. A.; Paholchuk, P. P.; Vasil'ev, E. A.; Kirichenko, A. N.; Gorevoy, A. V.; Rodionov, N. B. Intrapulse *in situ* Raman probing of electron, phonon and structural dynamics in synthetic diamond excited by ultrashort laser pulses: insights into atomistic structural damage. *Carbon* **2024**, *217*, No. 118606.
- (5) Apostolova, T.; Kurylo, V.; Gnilitskyi, I. Ultrafast laser processing of diamond materials: a review. *Front. Phys.* **2021**, *9*, 650280.
- (6) Tavella, F.; Höppner, H.; Tkachenko, V.; Medvedev, N.; Capotondi, F.; Golz, T.; Kai, Y.; Manfredda, M.; Pedersoli, E.; Prandolini, M. J.; Stojanovic, N.; Tanikawa, T.; Teubner, U.; Toleikis, S.; Ziaja, B. Soft x-ray induced femtosecond solid-to-solid phase transition. *High Energy Dens. Phys.* **2017**, *24*, 22–27.
- (7) Heimann, P.; Hartley, N. J.; Inoue, I.; Tkachenko, V.; Antoine, A.; Dorches, F.; Falcone, R.; Gaudin, J.; Höppner, H.; Inubushi, Y.; Kapcia, K. J.; Lee, H. J.; Lipp, V.; Martinez, P.; Medvedev, N.; Tavella, F.; Toleikis, S.; Yabashi, M.; Yabuuchi, T.; Yamada, J.; Ziaja, B. Non-thermal structural transformation of diamond driven by x-rays. *Struct. Dyn.* **2023**, *10* (5), No. 054502.
- (8) Medvedev, N.; Jeschke, H. O.; Ziaja, B. Nonthermal phase transitions in semiconductors induced by a femtosecond extreme ultraviolet laser pulse. *New J. Phys.* **2013**, *15*, No. 015016.
- (9) Medvedev, N.; Jeschke, H. O.; Ziaja, B. Nonthermal graphitization of diamond induced by a femtosecond x-ray laser pulse. *Phys. Rev. B* **2013**, *88* (22), No. 224304.
- (10) Medvedev, N.; Tkachenko, V.; Ziaja, B. Modeling of nonthermal solid-to-solid phase transition in diamond irradiated with femtosecond x-ray FEL pulse. *Contrib Plasma Phys.* **2015**, *55* (1), 12–34.
- (11) Lipp, V.; Tkachenko, V.; Stransky, M.; Aradi, B.; Frauenheim, T.; Ziaja, B. Density functional tight binding approach utilized to study x-ray-induced transitions in solid materials. *Sci. Rep.* **2022**, *12* (1), No. 1551.
- (12) Medvedev, N.; Volkov, A. E. Multitemperature atomic ensemble: nonequilibrium evolution after ultrafast electronic excitation. *Phys. Rev. E* **2024**, *110* (2), No. 024142.
- (13) Jeschke, H. O.; Garcia, M. E.; Bennemann, K. H. Microscopic analysis of the laser-induced femtosecond graphitization of diamond. *Phys. Rev. B* **1999**, *60* (6), R3701–R3704.
- (14) Craig, C. F.; Duncan, W. R.; Prezhdo, O. V. Trajectory surface hopping in the time-dependent Kohn-Sham approach for electron-nuclear dynamics. *Phys. Rev. Lett.* **2005**, *95* (16), No. 163001.
- (15) Tully, J. C. Perspective: nonadiabatic dynamics theory. *J. Chem. Phys.* **2012**, *137* (22), No. 22A301.
- (16) Shimojo, F.; Ohmura, S.; Mou, W.; Kalia, R. K.; Nakano, A.; Vashishta, P. Large nonadiabatic quantum molecular dynamics simulations on parallel computers. *Comput. Phys. Commun.* **2013**, *184* (1), 1–8.
- (17) Fonoberov, V. A.; Balandin, A. A. Excitonic properties of strained wurtzite and zinc-blende GaN/Al_xGa_{1-x}N quantum dots. *J. Appl. Phys.* **2003**, *94* (11), 7178–7186.
- (18) Shimamura, K.; Yuan, Z.; Shimojo, F.; Nakano, A. Effects of twins on the electronic properties of GaAs. *Appl. Phys. Lett.* **2013**, *103* (2), No. 022105.
- (19) Runge, E.; Gross, E. K. U. Density-functional theory for time-dependent systems. *Phys. Rev. Lett.* **1984**, *52* (12), 997–1000.
- (20) Yabana, K.; Sugiyama, T.; Shinohara, Y.; Otobe, T.; Bertsch, G. F. Time-dependent density functional theory for strong electromagnetic fields in crystalline solids. *Phys. Rev. B* **2012**, *85* (4), No. 045134.
- (21) Jestadt, R.; Ruggenthaler, M.; Oliveira, M. J. T.; Rubio, A.; Appel, H. Light-matter interactions within the Ehrenfest-Maxwell-Pauli-Kohn-Sham framework: fundamentals, implementation, and nano-optical applications. *Adv. Phys.* **2019**, *68* (4), 225–333.
- (22) Linker, T.; Nomura, K.; Aditya, A.; Fukushima, S.; Kalia, R. K.; Krishnamoorthy, A.; Nakano, A.; Rajak, P.; Shimmura, K.; Shimojo, F.; Vashishta, P. Exploring far-from-equilibrium ultrafast polarization control in ferroelectric oxides with excited-state neural network quantum molecular dynamics. *Sci. Adv.* **2022**, *8* (12), No. eabk2625.
- (23) Razakh, T. M.; Linker, T.; Luo, Y.; Kalia, R. K.; Nomura, K.; Vashishta, P.; Nakano, A. Accelerating quantum light-matter dynamics on graphics processing units. *Proceedings of the International Workshop on Parallel and Distributed Scientific and Engineering Computing; PDSEC, 2024*; Article 64, DOI: [10.1109/IPDPSW63119.2024.00176](https://doi.org/10.1109/IPDPSW63119.2024.00176).
- (24) Lee, C. W.; Schleife, A. Hot-electron-mediated ion diffusion in semiconductors for ion-beam nanostructuring. *Nano Lett.* **2019**, *19* (6), 3939–3947.
- (25) Shimojo, F.; Hattori, S.; Kalia, R. K.; Kunaseth, M.; Mou, W.; Nakano, A.; Nomura, K.-i.; Ohmura, S.; Rajak, P.; Shimamura, K.; Vashishta, P. A divide-conquer-recombine algorithmic paradigm for multiscale materials modeling. *J. Chem. Phys.* **2014**, *140* (18), No. 18A529.
- (26) Blochl, P. E. Projector augmented-wave method. *Phys. Rev. B* **1994**, *50* (24), 17953–17979.
- (27) Perdew, J. P.; Burke, K.; Ernzerhof, M. Generalized gradient approximation made simple. *Phys. Rev. Lett.* **1996**, *77* (18), 3865–3868.
- (28) Grimme, S.; Antony, J.; Ehrlich, S.; Krieg, H. A consistent and accurate ab initio parametrization of density functional dispersion correction (DFT-D) for the 94 elements H–Pu. *J. Chem. Phys.* **2010**, *132* (15), No. 154104.